



Application of gas/liquid two-phase flow in cross-flow microfiltration of oil-in-water emulsion; permeate flux and fouling mechanism analysis

Amir Fouladitajar, Farzin Zokaee Ashtiani*, Bardiya Valizadeh, Seyed Borhan Armand, Ramin Izadi

Department of Chemical Engineering, Amirkabir University of Technology, No. 424, Hafez Ave., Tehran, Iran, Tel. +98 9124990549; email: fouladi@aut.ac.ir (A. Fouladitajar); Tel. +98 21 6454 3124; Fax: +98 2166405847; email: zokaee@aut.ac.ir (F.Z. Ashtiani), Tel. +98 9166311046; email: b.valizadeh@aut.ac.ir (B. Valizadeh), Tel. +98 9173515159; email: borhan@aut.ac.ir (S.B. Armand), Tel. +98 9166514509; email: izadiramin@yahoo.com (R. Izadi)

Received 26 April 2014; Accepted 21 November 2014

ABSTRACT

The effects of gas–liquid two-phase flow regimes on permeate flux and fouling mechanisms were investigated in a gas sparging assisted microfiltration of oil-in-water emulsion. Different two-phase flow patterns were attained by introducing gas stream into the liquid phase. It was found that the permeate flux was increased due to disruption of the local deposited cake layer and concentration polarization as the gas velocity increased. Flux enhancement of up to 35% was observed at slug-flow pattern and it was also found that gas sparging is less efficient at high liquid velocities in which turbulence was high. Fouling mechanisms were examined through four individual blocking laws. Membrane resistance curves were used to find dominant fouling mechanism during filtration and as a result, cake formation showed the best agreement with the experimental data in flux decline prediction. The effect of oil droplets on the membrane surface, pore blockage, and accumulation of fouling layer were also analyzed through scanning electron microscopy images.

Keywords: Membrane; Two-phase flow; Oil-in-water emulsion; Fouling mechanism

1. Introduction

Large amounts of oily wastewater are produced daily by many industrial establishments which can cause great environmental impacts if it is not treated effectively. Environmental regulations mandate petrochemical, metalworking, automotive industries, etc. to treat their wastewater before discharge. Different methods have been used for wastewater treatment; however, they are not suitable for separation of oil-in-water emulsions especially when the oil droplets are

smaller than 20 μm [1–3]. Development of membrane technology during recent decades has shown promising capability for oily wastewater treatment [4–6].

Variety of membrane separation processes have been developed in order to rectify this problem; however, microfiltration has shown more efficient performance in separating oil droplets from stable oil-in-water emulsions [7–10]. It has been extensively studied during the past decade, but membrane fouling and permeate flux decline have always been challenging problems, limiting its applications. In order to resolve this problem, different techniques have been recently studied. Some studies have focused on

*Corresponding author.

membrane modification to prepare fouling resistance membranes [11–13] while others used feed pretreatment [14], dynamic filtration [15,16], and flow manipulation [17–21] to reduce fouling.

Among these methods, gas sparging technique has proved to reduce membrane fouling and flux decline due to effective disruption of concentration polarization and cake layer [22–25]. A two-phase flow by means of introducing air bubbles into the liquid can enhance shear stress on the membrane surface and yet does not pose any harm to the membrane which might have been formed by suspended solid particles [26–28]. The effect of bubble-flow pattern on reducing fouling resistance and enhancement of cross-flow microfiltration is reported in our previous work [29]. It has shown that the slug-flow pattern increases filtrate flux the most. Also, it was observed that in sparse bubbly flow, introducing gas into flow almost did nothing at high liquid velocities. Same results were also reported by Hwang and Wu [30] in which flux enhancement was more remarkable at lower velocity region. Chiu and James [31] reported that critical flux of two-phase flow was up to almost twice greater than that of single-phase flow. In addition, the slug-flow pattern has shown the best results. Increasing shear stress at the membrane surface exerted by air bubbles, dispersion of concentration polarization layer, and reducing concentration of cake layer caused the flux enhancement.

However, fouling phenomena have always been of interest and a major challenge in membrane processes. This is due to its complexity and dependency on process characteristics. On top of that, oily systems are more challenged due to the deformation and coalescence of oil droplets. Pore blocking due to deposition of oil droplets inside the membrane pores and on the membrane surface are responsible for fouling [32]. Varieties of fouling mechanisms have been proposed in order to determine the fouling behavior of oily systems.

The concept of blocking laws is first introduced by Hermans and Bredee. Later, constant pressure blocking laws were revised by Hermia [33] applicable to dead-end filtration. However, equivalent equations were obtained with appropriate modifications for cross-flow filtration [34]. Cake filtration, intermediate, standard, and complete pore blocking are different classical models that have been developed to characterize flux performance. Since these individual models have failed to predict fouling behavior in some cases, combined models have been used to provide better fits of experimental data [32,35,36].

Continuing our activities in this field, the present study is aimed at investigating the effect of gas sparging on fouling and flux decline in microfiltration of

oil-in-water emulsion. Different gas velocities have been used to establish different gas–liquid two-phase flow regimes to evaluate their effect on fouling phenomena and flux enhancement. Four kinds of individual blocking laws were used to study the effects of gas sparging on the fouling mechanism. Besides, effect of oil droplets on blocking of the membrane pores before and after cleaning have also been investigated through scanning electron microscopy (SEM) images where the provided fittings and model predictions were reconfirmed by the SEM images.

2. Theory

Four fouling models have been used to describe oil deposition in pores and/or on the membrane surface. The standard pore blocking model assumes cylindrical pores of the membranes in which oil droplets are deposited on the pore wall. Accumulation of oil droplets causes decline to the radius of the pores and consequently decreases the permeability. In the complete and intermediate pore blocking models, oil droplets block the entrance of the pores and a portion of pores are unavailable for the permeate flow, and consequently the available membrane area decreases. The cake filtration model occurs when a permeable cake layer accumulates on the membrane surface and increases the resistance to flow. Each model equation shown in Table 1 is presented by Koltuniewicz et al. [37] for cross-flow microfiltration. They all can be summarized to obtain a general equation:

$$J = J_0 \left[1 + k(2 - n)(AJ_0)^{2-n} t \right]^{\frac{1}{n-2}} \quad (1)$$

where k is the generalized filtration constant and the values of n , blocking index (constant), respectively, are 1.5, 1.0, and 0 correspond to standard pore blocking, intermediate pore blocking, and cake filtration [37]. For a constant transmembrane pressure filtration, the term AJ_0 is constant and they can be simplified as linear equations [38] also presented in Table 1. Eq. (1) can be written in term of membrane resistance for constant pressure filtration with transmembrane pressure ΔP ,

$$R = R_0 \left[1 + k(2 - n)(AJ_0)^{2-n} t \right]^{\frac{1}{2-n}} \quad (2)$$

where $R_0 = \Delta P/J_0$. Therefore, the first-order and second-order derivatives of R with respect to time, t , are written as follows:

Table 1
Fouling blocking laws and their linearized forms

Fouling mechanism	Flux equation	Linearized flux equation
Complete pore blocking	$J = J_0 \exp(-k_b t)$	$\ln(J^{-1}) = \ln(J_0^{-1}) + k_b t$
Standard pore blocking	$J = J_0 \left(1 + \frac{1}{2} K_s (AJ_0)^{0.5} t\right)^{-2}$	$J^{-0.5} = J_0^{-0.5} + k_s t$
Intermediate pore blocking	$J = J_0 (1 + K_i AJ_0 t)^{-1}$	$J^{-1} = J_0^{-1} + k_i t$
Cake filtration	$J = J_0 \left(1 + 2K_c (AJ_0)^2 t\right)^{-0.5}$	$J^{-2} = J_0^{-2} + k_c t$

$$\frac{dR}{dt} = R_0 k (AJ_0)^{2-n} \left[1 + k(2-n)(AJ_0)^{2-n} t\right]^{\frac{n-1}{2-n}} \quad (3)$$

$$\frac{d^2R}{dt^2} = R_0 k^2 (n-1)(AJ_0)^{4-2n} \left[1 + k(2-n)(AJ_0)^{2-n} t\right]^{\frac{2n-3}{2-n}} \quad (4)$$

Accordingly, useful results can be obtained by examining $R(t)$, $dR(t)/dt$, and $d^2R(t)/dt^2$ curves. It shows that all the terms in the right hand side of Eq. (4) are positive, except $(n-1)$. If $n > 1$ then $d^2R(t)/dt^2$ will be positive, meaning that $dR(t)/dt$ is a monotonic increasing function. In this case, one can conclude that standard pore blocking plays a major role. In contrast, if $n < 1$, $d^2R(t)/dt^2$ will be negative and the first derivative will be monotonic decreasing function. This implies that the cake filtration is the dominant mechanism. Similar to these, if the curve of $dR(t)/dt$ becomes flat ($n=0$), intermediate pore blocking model is of great importance in microfiltration.

3. Experimental

3.1. Feed preparation

To achieve a fine dispersed oil-in-water emulsion, the feed was prepared by mixing gasoil (Tehran Refinery) and surfactant with distilled water at a mixing rate of 12,000 rpm for 30 min. Polyoxyethylene (80) sorbitanmonooleate (Tween 80, Merck) was used as surfactant at concentration of 100 ppm. A 0.45 μm pore size hydrophilic polyvinylidene fluoride flat-sheet membrane (Millipore Co.) with 125 μm thickness and 70% porosity was used for microfiltration. COD analysis was done based on the standard method of EPA 410.4 which has been described in detail in previous work [32].

3.2. Experimental apparatus

Schematic diagram of the lab scale experimental apparatus is shown in Fig. 1(a). The stable emulsion

feed was held in a 10 L tank. A centrifugal recirculation pump, controlled by an inverter was used to deliver the feed to the membrane module and also provided the required constant operating pressure of the oil-in-water emulsion. Two needle valves were installed in the feed and retentate lines to adjust the fluid flow rate. Besides, the valve installed after the membrane module, can exert a backpressure along the membrane unit. AMBLD Instrument Company flow meter, calibrated for the present experiments, was utilized. Two pressure gauges (Wika, Germany) were used before and after the membrane module to determine the pressure drop and also to observe the line pressures varied from 0.5 to 2 bar. The required air flow was supplied by a 25 L compressor with adjustable gas velocity, equipped with both regulator and flow meter. Gas and liquid were mixed just before entering the module. The permeate flow was measured by a digital balance (Sartorius Model GE2120, Edgewood, NY) with the accuracy of 0.01 g connected to a computer. Permeate was collected and regularly returned to the storage tank to guarantee a constant feed concentration. The system was able to adjust and control the important operating parameters, including temperature, operating pressure, and liquid and gas velocity. The membrane module was specifically designed and fabricated from Plexiglas to observe gas-liquid two-phase flow regimes, Fig. 1(b). The dimension of module channel was 10 cm \times 5 cm \times 3 mm as length, width, and depth, respectively, providing 50 cm² active filtration area. More details about the module and the experimental procedure have been given in previous work [29].

4. Results and discussion

4.1. The effect of gas sparging on permeate flux

In order to investigate the effect of gas sparging on permeate flux, two sets of experiments were carried out with different gas and liquid flow rates ($Q_G = 0.25, 0.5, 0.75, 1, \text{ and } 2 \text{ L/min}$; $Q_L = 1 \text{ and } 3 \text{ L/min}$). Two liquid flow rates of 1 and 3 L/min were tested in

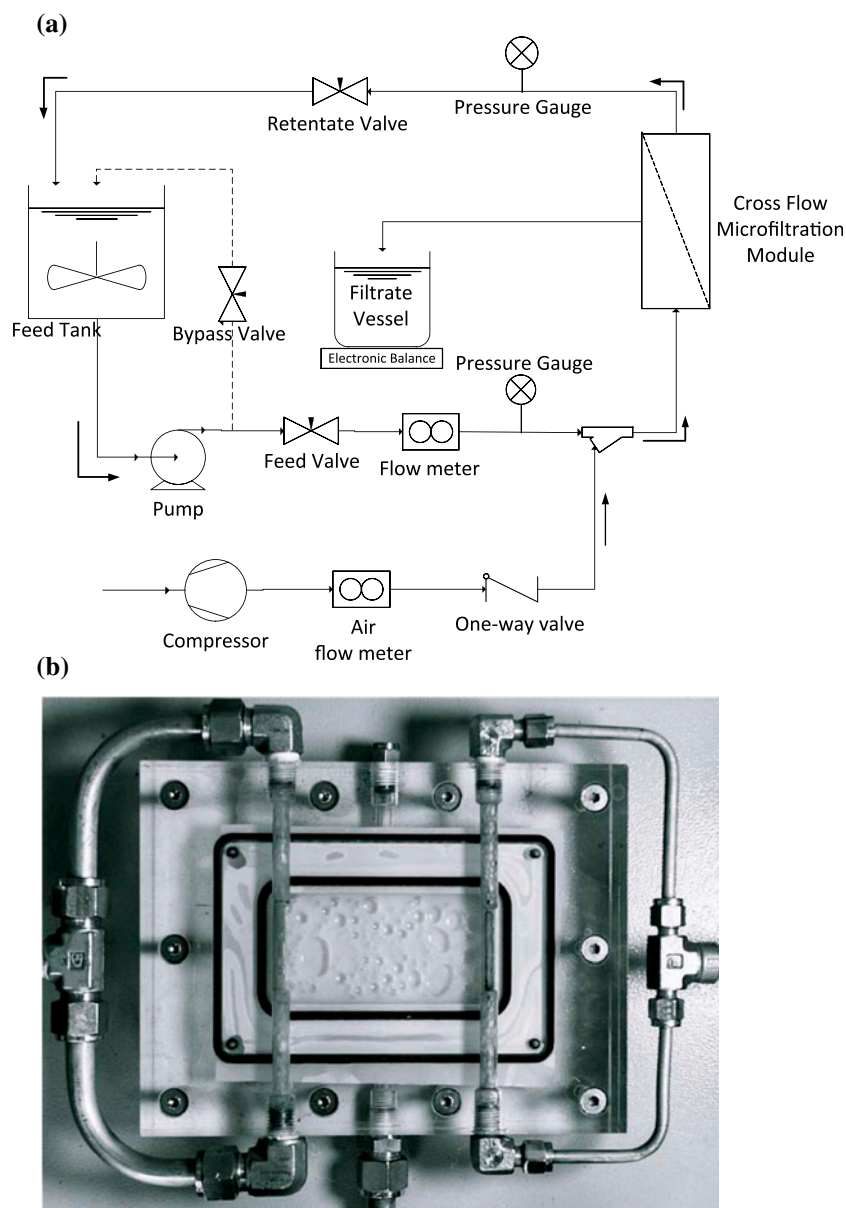


Fig. 1. (a) Schematic flow diagram of the membrane setup and (b) membrane module.

practice which are corresponded to 0.11 and 0.33 m/s, respectively. According to the module dimensions, these velocities resulted in Reynolds number of 700 and 2100, respectively. Depending on gas and liquid velocities, four distinct flow patterns, from bubbling to churn flow, were observed in the flat-sheet microfiltration module, shown in Fig. 2. Sparse bubbles were observed at low gas velocities which formed a dense uniform bubble flow as the gas velocity increased, Fig. 2(a, b). Then, slug-flow pattern was appeared at intermediate gas velocities, Fig. 2(c). Churn-flow

regime was observed at higher gas velocities ($Q_G=2$ L/min), Fig. 2(d). In higher gas velocities, the gas flow became dominant which resulted in annular flow being undesirable.

Fig. 3 shows the permeate flux decline for introducing different gas flow rates into the liquid where $Q_L=1$ L/min. The permeate flux decline was observed to be similar to most of the cross-flow microfiltration profiles. The main reason of the sharp decline at the early stage of filtration is resulted from the oil deposition on the membrane surface adding extra resistance.

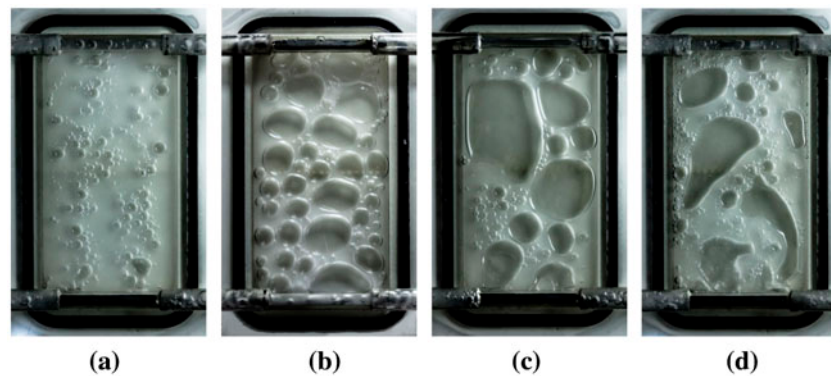


Fig. 2. Gas–liquid two-phase flow patterns in the flat-sheet microfiltration module for $Q_L = 1$ L/min and different gas flow rates: (a) sparse bubble $Q_G = 0.25$ L/min, (b) dense bubble $Q_G = 0.5$ L/min, (c) slug $Q_G = 0.75$ L/min, and (d) churn flow $Q_G = 2$ L/min.

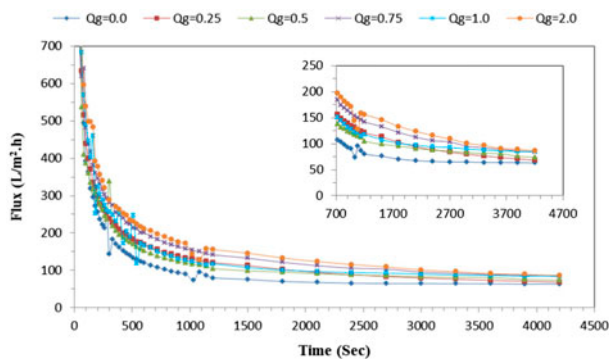


Fig. 3. Effect of gas–liquid two-phase flow on flux behavior at $Q_L = 1$ L/min, and room temperature (22 ± 1 °C).

Accordingly, by introducing gas into the liquid flow less flux decline is observed and final steady-state permeate flux is increased. Gas bubbles/slugs exert additional shear stress and increase turbulence, which disrupt the local deposited cake layer and/or concentration polarization. Consequently, gas sparging enhances permeate flux by reduction of external fouling and the higher the gas velocity, the higher the permeate flux will be.

As mentioned above, according to Fig. 3, increasing the bubble size had a positive impact on permeate flux enhancement by disrupting the local deposited cake layer and/or concentration polarization ($Q_G = 0.25$ and 0.5 L/min). Evidently, the effect of slug flow on reduction of external fouling and flux enhancement was quite considerable ($Q_G = 0.75$ and 1 L/min). Large bubbles with at least 1 cm diameter in slug flow cause reduction in cross-section availability of the liquid phase and also resulted a thin liquid film to remain on the membrane surface moving in

opposite direction. This phenomenon exerts high shear stress to the membrane wall which reduces external fouling. Same results were reported previously but only for two-phase flow regime in cylindrical module that slug flow was the most significant regime for permeate flux enhancement [39,40] which now is confirmed for flat-sheet module. Besides, churn-flow pattern did not make any significant enhancement in permeate flux in comparison with slug flow as it is shown in Table 2. Although its irregular and chaotic regime had increased permeate flux, it has not been recommended to assist membrane filtration. Same results were obtained for liquid flow rate of $Q_L = 3$ L/min. Increasing bubble size causes reduction of external fouling; as a result, the permeate flux was increased. The best performance was shown by the slug-flow regime which graphs were omitted due to similarity.

Table 2 includes flux enhancement for both liquid flow rates at different gas flow rates. Effect of different two-phase flow regimes mentioned above can also be seen here. In addition, it can be concluded that, although the final permeate flux is higher at the liquid flow rate $Q_L = 3$ L/min, the flux enhancement is lesser. This is due to the fact that turbulence in higher rates of liquid flow is high enough that gas bubbles cannot make a significant change in the local mass transfer layer above the membrane. So, gas sparging is a useful technique for manipulation of external resistances to reduce flux decline, however, at high liquid Reynolds numbers it is not efficient enough to make more turbulence which were discussed in detail in our previous work [29]. On the other hand, it showed a promising result that applying gas sparging to oil-in-water systems with less turbulence can significantly improve the permeate flux up to almost 35% at $Q_L = 1$ L/min.

Table 2
Final permeate flux and flux enhancement at different gas velocity

Gas flow rate Q_G (L/min)	Liquid flow rate $Q_L = 1$ L/min		Liquid flow rate $Q_L = 3$ L/min	
	Final permeate flux (L/m ² h)	Flux enhancement (%)	Final permeate flux (L/m ² h)	Flux enhancement (%)
0	63.12	0	70	0
0.25	68.14	7.9	72.8	4
0.5	73.82	17	77.1	10
0.75	83.83	32.8	86.7	23.9
1	84.96	34.6	88.15	25.9
2	86.33	36.8	90.4	29.1

4.2. Analysis of fouling mechanisms

The fouling mechanisms discussed in Section 2 were tested in different operating conditions to reveal the relation between the variables and dominant mechanisms. In fact, this is the first time that individual blocking laws were applied in gas-sparged microfiltration of oil-in-water emulsion to predict the filtration flux. The correlation of four filtration models for a specific operating condition (TMP = 1 bar, $C_{oil} = 10,000$ mg/L, $Q_L = 1$ L/min, and $Q_G = 0.75$ L/min) has been depicted in Fig. 4(a). Except the cake filtration model, the other three models did not exhibit a reasonable agreement with experimental data giving non-linear correlations. Using the models' correlations for each case, a comparison was also made with the experimental data. As shown in Fig. 4(b), the cake formation model showed the best agreement with the experimental data, while the other tested models failed to provide any appropriate fitting. The same fouling behavior has been observed and reported in microfiltration of feeds containing solid particles [35]. It should be also noted that the cake filtration model tends to underestimate the initial flux, while the other models give an acceptable amount for the initial flux.

In addition, variations in the membrane resistance (R) and its first-order derivative with respect to time, (dR/dt), were also used to analyze the fouling mechanisms as a function of filtration time, Fig. 5. The membrane resistance gradually increased during microfiltration. The curve of dR/dt , however, was roughly composed of two regions; first a sharp decreasing region in the initial period of filtration and then a slow decline. This indicates that because of the sharp negative slope the cake filtration model was the major mechanism at the early stage of microfiltration. It also reveals quick development of oil cake on the surface of the membrane which corroborates the previous discussion. As the filtration time went on, the cake filtration was still the major mechanism, but

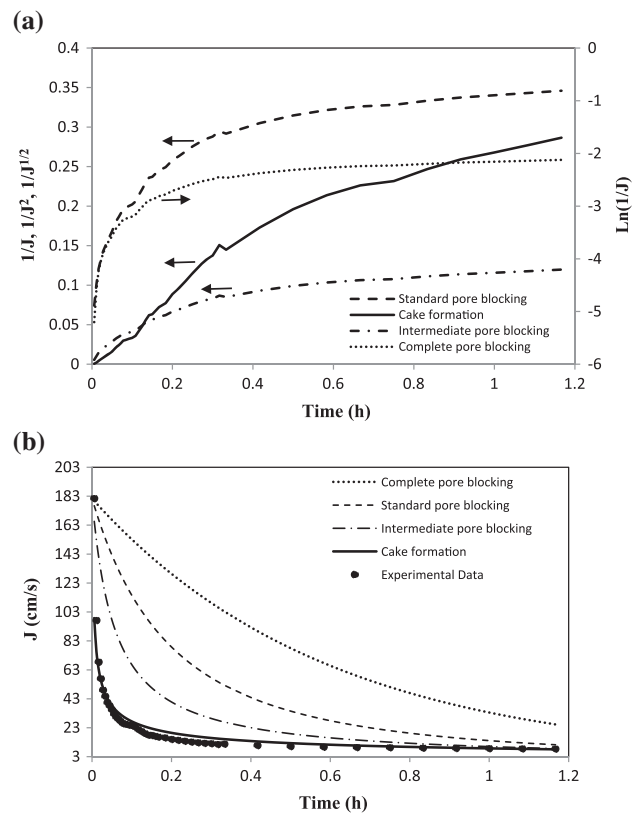


Fig. 4. (a) Variation of flux functions with time for four filtration models; (b) comparison of filtration model prediction with experimental data at oil concentration and TMP of 10,000 mg/L and 1 bar, respectively.

according to the slope of the curve, the rate of cake formation became slower. No obvious intermediate, complete, or standard pore fouling stages were observed.

The performance data for some other operating conditions were analyzed in the same way. Although the liquid and gas flow rate could improve the permeate flux, it was found that their influence on the

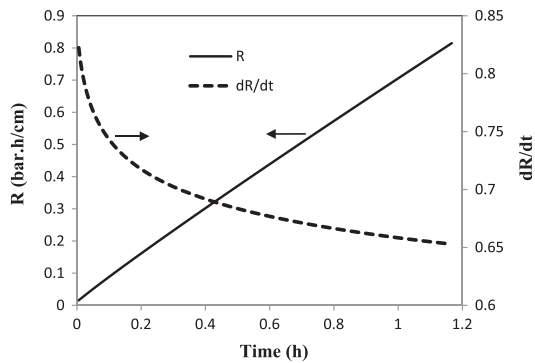


Fig. 5. Membrane resistance data and dR/dt analysis at oil concentration and TMP of 10,000 mg/L and 1 bar, respectively.

fouling mechanisms was negligible in comparison with the oil concentration and TMP. As long as the oil concentration and TMP were kept constant, almost the same results as above were obtained; therefore, their graphs were omitted due to similarity.

As the oil concentration decreased and TMP increased to 1,000 mg/L and 2 bar, respectively, a quite different behavior was observed. Fig. 6(a) shows that there is not a single linear correlation of the data over the complete range of filtration times. As depicted, there appears two filtration regions, one at the early stages (<5 min) and the other >5 min. By using the models correlations for each case a comparison was made with the experimental data (Fig. 6(b)). It is worth mentioning that when a mechanism dominates during filtration time, applying combined pore blocking laws usually do not offer much more benefit over the individual models [32,36]. It is evident from the graph that the cake filtration model is still better than the other models, but its outcome is not basically satisfying in the whole period.

The experimental data was therefore analyzed separately in the two time ranges. The linear correlations of the fouling models in the early stages of filtration time have been shown in Fig. 7(a). As illustrated, reasonable linear correlations have been achieved for this short period. The ability of the obtained correlations to predict permeate flux as a function of time has been plotted in Fig. 7(b). It can be seen that cake formation and intermediate pore blocking model have provided better fits where the other two predictions by standard and complete pore blocking were not appropriate.

Fig. 8(a) shows the correlation of the filtration models for longer filtration times in which an almost reasonable and linear correlation exists. The corresponding flux predictions vs. time were obtained from the model correlations and are shown in Fig. 8(b). As

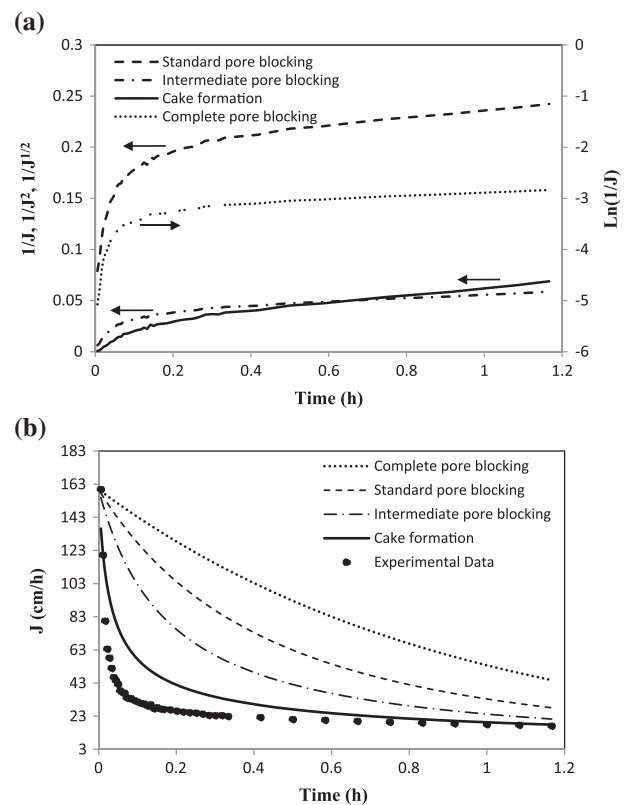


Fig. 6. (a) Variation of flux functions with time for four filtration models; (b) comparison of filtration model prediction with experimental data at oil concentration and TMP of 1,000 mg/L and 2 bar, respectively.

it shows, the complete and standard pore models were inappropriate, while the cake filtration and intermediate pore blocking models appear to provide better fits of the data. This implies that at the early stage, a cake layer of the oil droplets have been developed on the membrane surface which has protected the membrane pores of being blocked. As before, the cake filtration mechanism predominated at the beginning of the process and was the dominant fouling mechanism. At this period, the pores may behave as those in a fresh one. In longer times, the high transmembrane pressure can force the deformable droplets to seal off the pores. The oil droplets therefore will block the entrance of the pores and make them unavailable to the flow. This reveals that the intermediate pore blocking have played a major role in longer filtration times.

Fig. 9 reconfirm the above-mentioned states where membrane resistance and its derivative have been plotted versus time. As depicted, membrane resistance gradually increased during the process. Its derivative (dR/dt), however, decreased sharply at the beginning and then became flat. According to what was stated in

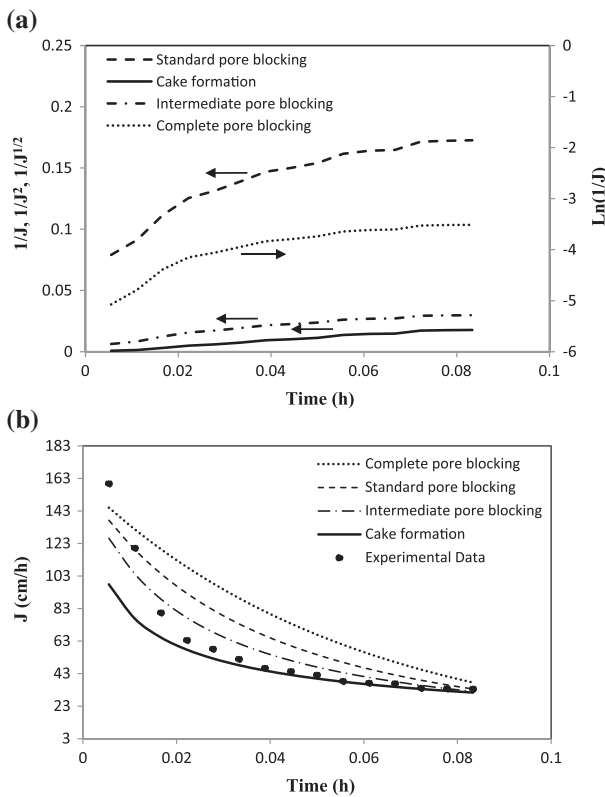


Fig. 7. (a) The linear correlations of pore blocking models; (b) comparison of filtration model prediction with experimental data at the early stages of filtration time.

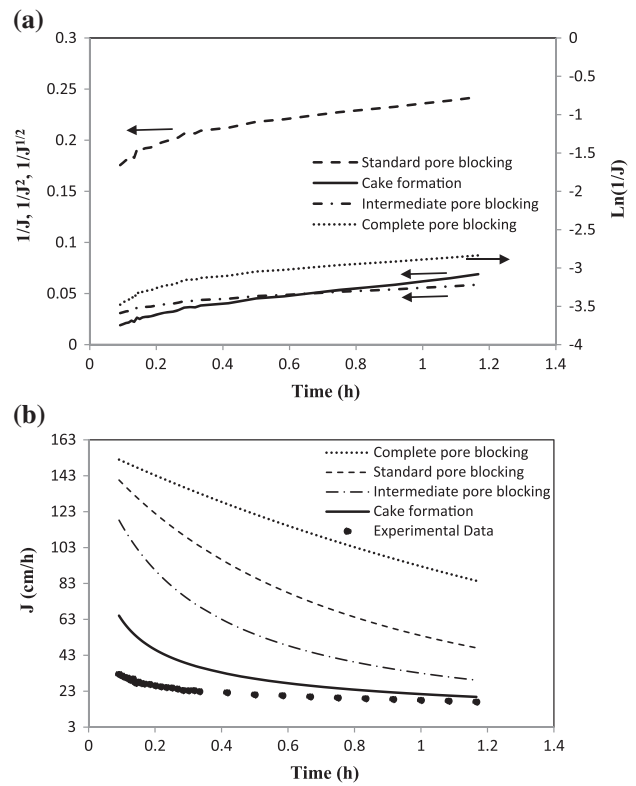


Fig. 8. (a) The linear correlations of pore blocking models; (b) comparison of filtration model prediction with experimental data at long filtration time.

Section 2, minus slope and flat curve, respectively, correspond to the cake filtration and intermediate fouling models.

4.3. Assessment of membrane fouling by SEM

SEM was used to estimate the effect of emulsion filtration on the membrane surface and the accumulation of any fouling layer. SEM of the new membrane as well as the used one (before and after cleaning) has been shown in Fig. 10. Fig. 10(a) indicates the pores of a new membrane sample which are clear. After running microfiltration of oil-in-water emulsion, most of the pores were clogged and the oil droplets partially occupied most of the pores (Fig. 10(b)). When only water was applied as the cleaning agent, the oil deposited layer on the membrane surface was almost disrupted, but the fouled pores were hardly cleaned (Fig. 10(c)). Finally, when applying caustic and acidic chemical cleaning solutions, a majority of the pores were cleaned (Fig. 10(d)). A 0.2 wt.% NaOH and 0.1 wt.% HNO₃ for 45 min and 30 min were used for chemical cleaning, respectively. This procedure was

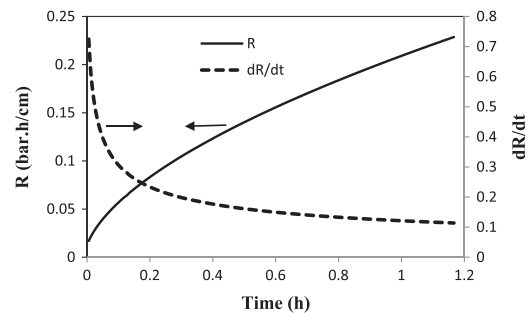


Fig. 9. Membrane resistance data and dR/dt analysis at oil concentration and TMP of 1,000 mg/L and 2 bar, respectively.

used according to the recommendation of the manufacturer. A portion of the membrane fouling during oil-in-water microfiltration was not reversible as attempts to clean the membrane using the mentioned chemical cleaning solutions did not remove all the oil deposits, as depicted in Fig. 10(d). It shows that although the majority of the occupied pores have been cleaned, there are still some deposited oil droplets which imply the intermediate pore blocking.

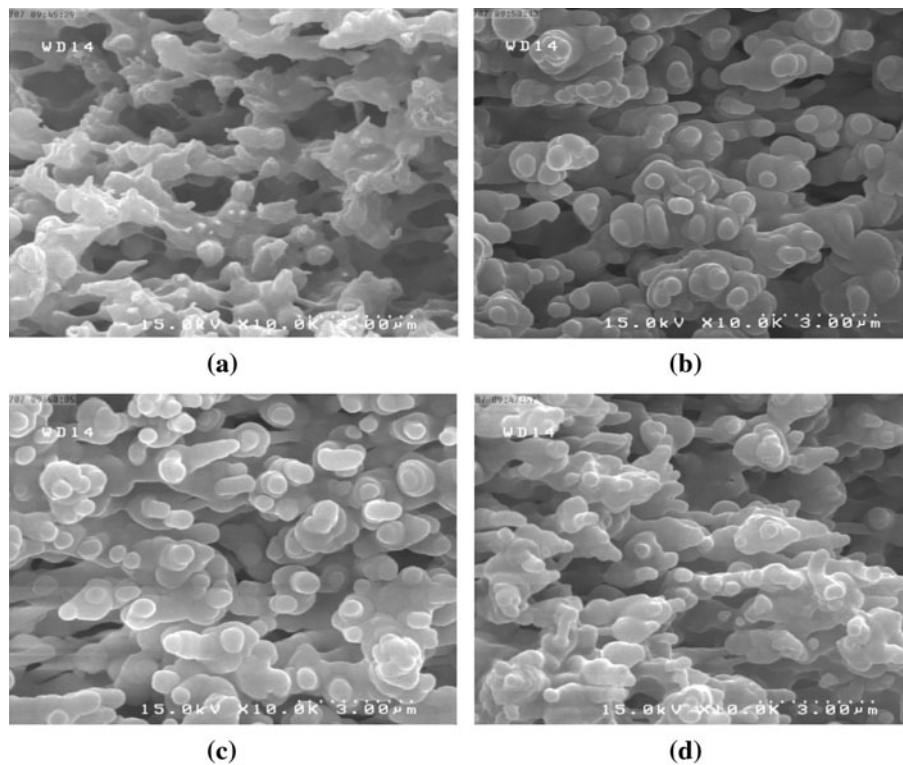


Fig. 10. Effect of emulsion filtration and chemical cleaning on the membrane surface: (a) new membrane, (b) after microfiltration of oil-in-water emulsion, (c) after cleaning by water, and (d) after chemical cleaning.

5. Conclusions

Gas sparging effect in microfiltration of oil-in-water emulsion was investigated. Gas bubbles with different velocities were injected into the liquid flow to obtain various gas/liquid two-phase flow patterns. It was found that shear stress exerted by enlarged gas bubbles had a positive impact on permeate flux enhancement. Increasing gas velocity increased permeate flux by reduction of external fouling. Since the turbulence was high enough at high liquid velocities, the bubbles were less efficient in disruption of mass transfer boundary layer on the membrane surface. Therefore, gas sparging was found to be a useful technique especially at low liquid velocities.

Four fouling resistance models were investigated to predict the permeate flux decline during filtration. It was concluded that cake formation is in better agreement with experimental data among others which failed to provide any appropriate fitting. However, cake formation had lower initial flux while other models gave acceptable amounts for the initial flux. Using membrane resistance curves, it was also supported that cake formation was the dominant fouling mechanism during filtration. Comparison of SEM of

the new membrane with the used ones (before and after cleaning) showed that a portion of the membrane fouling during oil-in-water microfiltration was not reversible as attempts to clean the membrane did not remove all oil deposits.

Acknowledgments

The Authors are gratefully thankful to Pars Oil and Gas Company (POGC) for their financial support (contract No. PT/91-177).

Symbols

J	—	permeate flux
J_0	—	initial permeate flux at time $t = 0$
K	—	constant in generalized model
N	—	blocking index
A	—	membrane area
T	—	filtration time
ΔP	—	transmembrane pressure
R	—	membrane resistance
R_0	—	initial membrane resistance at time $t = 0$

References

- [1] J. Zhong, X. Sun, C. Wang, Treatment of oily wastewater produced from refinery processes using flocculation and ceramic membrane filtration, *Sep. Purif. Technol.* 32 (2003) 93–98.
- [2] M. Zare, F. Zokaee Ashtiani, A. Fouladitajar, CFD modeling and simulation of concentration polarization in microfiltration of oil–water emulsions; Application of an Eulerian multiphase model, *Desalination* 324 (2013) 37–47.
- [3] Y.S. Li, L. Yan, C.B. Xiang, L.J. Hong, Treatment of oily wastewater by organic–inorganic composite tubular ultrafiltration (UF) membranes, *Desalination* 196 (2006) 76–83.
- [4] P. Janknecht, A.D. Lopes, A.M. Mendes, Removal of industrial cutting oil from oil emulsions by polymeric ultra- and microfiltration membranes, *Environ. Sci. Technol.* 38 (2004) 4878–4883.
- [5] B. Chakrabarty, A.K. Ghoshal, M.K. Purkait, Ultrafiltration of stable oil-in-water emulsion by polysulfone membrane, *J. Membr. Sci.* 325 (2008) 427–437.
- [6] K. Masoudnia, A. Raisi, A. Aroujalian, M. Fathizadeh, Cross-flow microfiltration oil-in-water emulsion using polyvinylidene fluoride membrane, *Procedia Eng.* 44 (2012) 1974–1976.
- [7] A. Ezzati, E. Gorouhi, T. Mohammadi, Separation of water in oil emulsions using microfiltration, *Desalination* 185 (2005) 371–382.
- [8] Y. Wang, X. Chen, J. Zhang, J. Yin, H. Wang, Investigation of microfiltration for treatment of emulsified oily wastewater from the processing of petroleum products, *Desalination* 249 (2009) 1223–1227.
- [9] H. Lotfiyan, F.Z. Ashtiani, A. Fouladitajar, Computational fluid dynamics modeling and experimental studies of oil-in-water emulsion microfiltration in a flat sheet membrane using Eulerian approach, *J. Membr. Sci.* 472 (2014) 1–9.
- [10] A. Fouladitajar, F.Z. Ashtiani, B. Dabir, H. Rezaei, B. Valizadeh, Response surface methodology for the modeling and optimization of oil-in-water emulsion separation using gas sparging assisted microfiltration, *Environ. Sci. Pol. Res.* (2014), doi: [10.1007/s11356-014-3511-6](https://doi.org/10.1007/s11356-014-3511-6).
- [11] J.-E. Zhou, Q. Chang, Y. Wang, J. Wang, G. Meng, Separation of stable oil–water emulsion by the hydrophilic nano-sized ZrO₂ modified Al₂O₃ microfiltration membrane, *Sep. Purif. Technol.* 75 (2010) 243–248.
- [12] I. Sadeghi, A. Aroujalian, A. Raisi, B. Dabir, M. Fathizadeh, Surface modification of polyethersulfone ultrafiltration membranes by corona air plasma for separation of oil/water emulsions, *J. Membr. Sci.* 430 (2012) 24–36.
- [13] W. Chen, J. Peng, Y. Su, L. Zheng, L. Wang, Z. Jiang, Separation of oil/water emulsion using Pluronic F127 modified polyethersulfone ultrafiltration membranes, *Sep. Purif. Technol.* 66 (2009) 591–597.
- [14] X. Qiao, Z. Zhang, J. Yu, X. Ye, Performance characteristics of a hybrid membrane pilot-scale plant for oil-field-produced wastewater, *Desalination* 225 (2008) 113–122.
- [15] M.Y. Jaffrin, Dynamic shear-enhanced membrane filtration: A review of rotating disks, rotating membranes and vibrating systems, *J. Membr. Sci.* 324 (2008) 7–25.
- [16] M.E. Ersahin, H. Ozgun, R.K. Dereli, I. Ozturk, K. Roest, J.B. van Lier, A review on dynamic membrane filtration: Materials, applications and future perspectives, *Bioresour. Technol.* 122 (2012) 196–206.
- [17] J. Cakl, I. Bauer, P. Dolecek, P. Mikulasek, Effects of backflushing conditions on permeate flux in membrane crossflow microfiltration of oil emulsion, *Desalination* 127 (2000) 189–197.
- [18] R.G. Holdich, I.W. Cumming, I.D. Smith, Cross flow microfiltration of oil in water dispersions using surface filtration with imposed fluid rotation, *J. Membr. Sci.* 143 (1998) 263–274.
- [19] J.-P. Kim, J.-J. Kim, B.-R. Min, K.Y. Chung, J.-H. Ryu, Effect of glass ball insertion on vortex-flow microfiltration of oil-in-water emulsion, *Desalination* 143 (2002) 159–172.
- [20] K. Scott, R.J. Jachuck, D. Hall, Crossflow microfiltration of water-in-oil emulsions using corrugated membranes, *Sep. Purif. Technol.* 22–23 (2001) 431–441.
- [21] Z. Jalilvand, F.Z. Ashtiani, A. Fouladitajar, Computational fluid dynamics modeling and experimental study of continuous and pulsatile flow in flat sheet microfiltration membranes, *J. Membr. Sci.* 450 (2014) 207–214.
- [22] W. Youravong, Z. Li, A. Laorko, Influence of gas sparging on clarification of pineapple wine by microfiltration, *J. Food Eng.* 96 (2010) 427–432.
- [23] J.Q.J.C. Verberk, J.C. van Dijk, Air sparging in capillary nanofiltration, *J. Membr. Sci.* 284 (2006) 339–351.
- [24] H. Fadaei, S.R. Tabaei, R. Roostaazad, Comparative assessment of the efficiencies of gas sparging and back-flushing to improve yeast microfiltration using tubular ceramic membranes, *Desalination* 217 (2007) 93–99.
- [25] N. Javadi, F.Z. Ashtiani, A. Fouladitajar, A. Mousavi, Experimental studies and statistical analysis of membrane fouling behavior and performance in microfiltration of microalgae by a gas sparging assisted process, *Bioresour. Technol.* 162 (2014) 350–357.
- [26] C. Cabassud, S. Laborie, L. Durand-Bourlier, J.M. Lainé, Air sparging in ultrafiltration hollow fibers: Relationship between flux enhancement, cake characteristics and hydrodynamic parameters, *J. Membr. Sci.* 181 (2001) 57–69.
- [27] Z.F. Cui, S. Chang, A.G. Fane, The use of gas bubbling to enhance membrane processes, *J. Membr. Sci.* 221 (2003) 1–35.
- [28] A. Drews, H. Prieske, E.-L. Meyer, G. Senger, M. Kraume, Advantageous and detrimental effects of air sparging in membrane filtration: Bubble movement, exerted shear and particle classification, *Desalination* 250 (2010) 1083–1086.
- [29] A. Fouladitajar, F. Zokaee Ashtiani, H. Rezaei, A. Haghmoradi, A. Kargari, Gas sparging to enhance permeate flux and reduce fouling resistances in cross flow microfiltration, *J. Ind. Eng. Chem.* 20 (2013) 624–632.
- [30] K.-J. Hwang, Y.-J. Wu, Flux enhancement and cake formation in air-sparged cross-flow microfiltration, *Chem. Eng. J.* 139 (2008) 296–303.

- [31] T. Chiu, A. James, Critical flux enhancement in gas assisted microfiltration, *J. Membr. Sci.* 281 (2006) 274–280.
- [32] A. Fouladitajar, F. Zokaee Ashtiani, A. Okhovat, B. Dabir, Membrane fouling in microfiltration of oil-in-water emulsions; a comparison between constant pressure blocking laws and genetic programming (GP) model, *Desalination* 329 (2013) 41–49.
- [33] J. Hermia, Constant pressure blocking filtration laws-application to power-law non-Newtonian fluids, *Trans. IChemE* 60 (1982) 183–187.
- [34] T.C. Arnot, R.W. Field, A.B. Koltuniewicz, Cross-flow and dead-end microfiltration of oily-water emulsions Part II. Mechanisms and modelling of flux decline, *J. Membr. Sci.* 169 (2000) 1–15.
- [35] H. Rezaei, F.Z. Ashtiani, A. Fouladitajar, Effects of operating parameters on fouling mechanism and membrane flux in cross-flow microfiltration of whey, *Desalination* 274 (2011) 262–271.
- [36] G. Bolton, D. Lacasse, R. Kuriyel, Combined models of membrane fouling: Development and application to microfiltration and ultrafiltration of biological fluids, *J. Membr. Sci.* 277 (2006) 75–84.
- [37] A.B. Koltuniewicz, R.W. Field, T.C. Arnot, Cross-flow and dead-end microfiltration of oily-water emulsion. Part I: Experimental study and analysis of flux decline, *J. Membr. Sci.* 102 (1995) 193–207.
- [38] B. Hu, K. Scott, Microfiltration of water in oil emulsions and evaluation of fouling mechanism, *Chem. Eng. J.* 136 (2008) 210–220.
- [39] M. Mercier, C. Fonade, C. Lafforgue-Delorme, How slug flow can enhance the ultrafiltration flux in mineral tubular membranes, *J. Membr. Sci.* 128 (1997) 103–113.
- [40] C. Cabassud, S. Laborie, J.M. Laine, How slug flow can improve ultrafiltration flux in organic hollow fibers, *J. Membr. Sci.* 128 (1997) 93–101.